Gunn DA, Chambers JE, Uhlemann S, Wilkinson PB, Meldrum PI, Dijkstra TA, Haslam E, Kirkham M, Wragg J, Holyoake S, Hughes PN, Hen-Jones R, Glendinning S. Moisture monitoring in clay embankments using electrical resistivity tomography. *Constuction and Building Materials* 2015, 92, 82-94.

Construction and Building Materials 92 (2015) 82–94

Contents lists available at ScienceDirect

Construction and Building Materials

journal homepage: www.elsevier.com/locate/conbuildmat

Moisture monitoring in clay embankments using electrical resistivity tomography

D.A. Gunn [a,*], J.E. Chambers [a], S. Uhlemann [a,c], P.B. Wilkinson [a], P.I. Meldrum [a], T.A. Dijkstra [a], E. Haslam [a], M. Kirkham [a], J. Wragg [a], S. Holyoake [a], P.N. Hughes [d], R. Hen-Jones [b], S. Glendinning [b]

[a] British Geological Survey, Nottingham NG12 5GG, UK
[b] School of Civil Engineering and Geosciences, Newcastle University, Newcastle upon Tyne NE1 7RU, UK
[c] ETH Zurich, Institute of Geophysics, Sonneggstrasse 5, 8092 Zurich, Switzerland
[d] School of Engineering and Computer Sciences, Durham University, DH1 3LE, UK

HIGHLIGHTS

- New remote monitoring technologies/approaches.
- Proactive maintenance using subsurface images.
- Increased time for early interventions.

ARTICLE INFO

Article history:
Received 2 February 2014
Accepted 5 June 2014
Available online 16 July 2014

Keywords:
Resistivity
Embankments
Moisture
Railway

ABSTRACT

Systems and methods are described for monitoring temporal and spatial moisture content changes in clay embankments using electrical resistivity tomography (ERT) imaging. The methodology is based upon development of a robust relationship between fill resistivity and moisture content and its use in the transformation of resistivity image differences in terms of relative moisture content changes. Moisture level and moisture content movement applications are exemplified using two case histories from the UK. The first is the BIONICS embankment, near Newcastle (NE England), which was constructed in 2005 using varying degrees of compaction of a medium plasticity sandy, silty clay derived from the Durham Till. The second is a Victorian embankment south of Nottingham (Central England), constructed in 1897 using end tipping of Late Triassic siltstone and mudstone taken from local cuttings. Climate change forecasts for the UK suggest that transportation earthworks will be subjected to more sustained, higher temperatures and increased intensity of rainfall. Within the context of preventative geotechnical asset maintenance, ERT imaging can provide a monitoring framework to manage moisture movement and identify failure trigger conditions within embankments, thus supporting on demand inspection scheduling and low cost early interventions.

1. Introduction

Engineered slopes, embankments, canals, earth dams, sea walls and flood defences are increasingly susceptible to catastrophic failure due to changes in global climatic conditions and land use. The 4th Assessment Report of the Intergovernmental Panel on Climate Change [23,24] predicted that mid- to high-latitude regions can expect more extreme events with up to 20% more precipitation, more flash floods, and a rise in sea levels up to 59 cm by the end of the century. The predicted environmental changes will have inevitable consequences for the serviceability and maintenance of our engineered infrastructure, but while the impact is still largely unknown, we require intelligent platforms and science to monitor current condition and assess risk over the whole life cycle of UK assets. Aged assets include: Canal & River Trust/Scottish Canals with 3450 km of aged canal earthworks, Network Rail with over 20,000 km of earthwork embankments and cuttings, and London Underground with 236 km of embankments and cuttings in Greater London, all contributing significantly to the UK economy.

A significant number of UK earthworks between 100 and 200 years old were constructed using tipping methods, which was standard in the 19th century. This has left a legacy of ageing, highly fissured, weak and heterogeneous earth structures, which are still intensively used but prone to failure under aggressive climatic stresses [28]. Common problems in certain subgrade soil types include

* Corresponding author.
E-mail address: dgu@bgs.ac.uk (D.A. Gunn).

http://dx.doi.org/10.1016/j.conbuildmat.2014.06.007
0950-0618/

shear failure and mud pumping caused by loss of strength and cohesion [33,25], heave, deformation and the formation of ballast pockets [31,5], which also occur in zones of low density and stiffness. In most cases, subgrade problems are associated with high moisture levels, a key factor in reducing consistency and strength, and ultimately leading to failure [32,18].

Modelling undertaken during the recently completed FUTURENET project [3,4] showed how climate or weather event sequences affect the traffic capacity of transportation networks. Weather events have direct effects on the permanent way such as increased temperature on risk of track buckling (or pavement rutting) and related effects on potential failure of the subgrade and surrounding ground including landslide, shrink–swell and scour. Climate resilience planning for transportation networks requires access to near real-time, volumetric, and hence holistic, assessment of infrastructure condition, including ground water movement and the moisture levels within the earthworks asset. Maintenance practice, based primarily on surface observations, is a barrier to proactive approaches because these represent the latter stages of failure and reinforce responsive solutions. Risk-based prevention and early interventions require identification of the incremental development of internal conditions that ultimately trigger failure. Key to this process will be adaptive technologies delivering real-time images of the true 3D spatial variation of groundwater and geotechnical properties affecting stability. While providing useful ground truth, a full understanding of vital ground processes with sufficient temporal and spatial resolution is often not possible from invasive investigation alone. We assert that this role can be filled by non-invasive geophysical methods that not only provide real-time images of moisture movement but are also calibrated so as to indicate full 3D, quantitative geotechnical property changes. This can be achieved if the geophysical relationships between electrical resistivity and geotechnical properties (such as moisture content, pore pressure and strength) are well understood.

Resistivity imaging, or electrical resistivity tomography (ERT), is sensitive to lithological and mineralogical heterogeneity [34] and changes in ground temperature and soil moisture content [10,11,19,12]. In locations where lithology and mineralogy are unchanged, provided ground temperature effects can be corrected, changes in successive ERT surveys over an electrode array of constant geometry and location will be due to ground water movement and subsequent moisture content variations. Thus, by applying appropriate temperature correction and petrophysical relationships linking resistivity and saturation [7,6,12], time-lapse, volumetric (4D) images of water movement and moisture content changes can be constructed from repeated ERT surveys. Alongside the increased use of ERT in site investigation, purpose built ERT monitoring instrumentation has rapidly developed and now incorporates telemetric control and automatic data transfer, scheduling, and processing [30]. This type of instrumentation is now being applied to monitor of natural slopes [27,37,35] and transportation earthworks [19,12].

In this study we describe repeat survey-based approaches using standard field equipment/return visits and fully automated monitoring and data capture on permanent field installations to investigate the structure and processes in sections of two embankments. We provide two case histories: firstly, from the BIONICS research embankment, Nafferton Farm, Northumberland, UK [14,21] constructed using varying amounts of compaction in 2005 from sandy, silty clay derived from partially sorted Durham Till; which includes identification of individual lifts from 2D resistivity sections across the embankment transect; and secondly, from an embankment along the former Great Central Railway near East Leake, Nottingham, UK [2,17,19] constructed via end-tipping of materials derived from the East Leake Tunnel cutting to the south; which includes identification of fill regime changes in a 2D resistivity section along the axis of the embankment, dynamic, seasonal wetting and drying fronts moving through a 2D transect of the embankment and a demonstration of the potential application of 3D volumetric images of moisture movement and geotechnical property visualisation for planning maintenance. Finally, these case histories provide the context for a broad discussion relating to the foundation for new risk-based asset management practices incorporating automated, electrical imaging technologies into early intervention decision processes, such as proactive drainage planning.

2. Soil and rock resistivity

2.1. Resistivity measurements and field systems

Fig. 1a shows that the resistivity, ρ_s of a unit volume of material is given as,

$$\rho_s = \frac{V}{I} \cdot \frac{A}{L} \tag{1}$$

where $\frac{V}{I}$ is the ratio of the difference, V in the electrical potential at the two opposing faces of a unit cube that are orthogonal to the current flow, I and is equivalent to the material resistance, R and $\frac{A}{L}$ is the Geometric Factor (in Fig. 1a) that accounts for how the current flow within the material and the measurement are affected by the electrode geometry, and converts resistance R to resistivity, ρ_s.

Resistivity is measured in the field using a four-electrode array consisting of two current injection electrodes and two potential measurement electrodes. In general, the depth of investigation increases with increasing electrode separation, where the different electrode array configurations determine the specific relationship. For example, Fig. 1b shows how the depth of investigation for a dipole–dipole array is related to the common spacing (denoted 'a') between the current and potential electrode pairs. It also shows how a 2D 'apparent resistivity' section along a transect can be constructed from a series of resistivity measurements at different inter-dipole spacings (denoted 'n'). Further processing can also be undertaken to refine these images to produce the best estimate of the true ground resistivity distribution; a process termed 'inversion'. The ABEM SAS 1000 is typical of the field equipment used to make resistivity-depth soundings or 2D cross-sectional surveys. A series of field measurements are made, usually by varying the electrode spacing in standard four-electrode array configurations, such as the dipole–dipole (or Wenner or Schlumberger) arrays, from which apparent resistivity sections are constructed. The voltage measurement between two potential electrodes can be considered as a single channel. As surveys require multiple measurements, the duration of the survey can be reduced by an equivalent factor to the number of channels used.

Datasets for 3D imaging typically require many thousands of four-electrode measurements over a range of geometries to be carried out across the area of interest. Thus, equipment with lower numbers of input channels are disadvantaged by longer survey times. The AGI SuperSting R8 is typical of field equipment used for 3D surveys, boasting eight channels with the potential to connect up to 65,000 electrodes, (although most surveys don't utilise anywhere near this potential but the eight channel system reduces surveying times). 3D apparent resistivity images, or models of the true resistivity distribution in the subsurface are constructed from the measured resistivity dataset, in a similar manner to the multi-point construction in 2D surveys (Fig. 1c). The new generation of remote monitoring platforms such as the Automated time-Lapse Electrical Resistivity Tomography (ALERT) and the very recent Proactive Infrastructure Monitoring and Evaluation (PRIME) systems combine emerging electrical resistivity imaging technology with wireless telecommunications, server-based processing, site

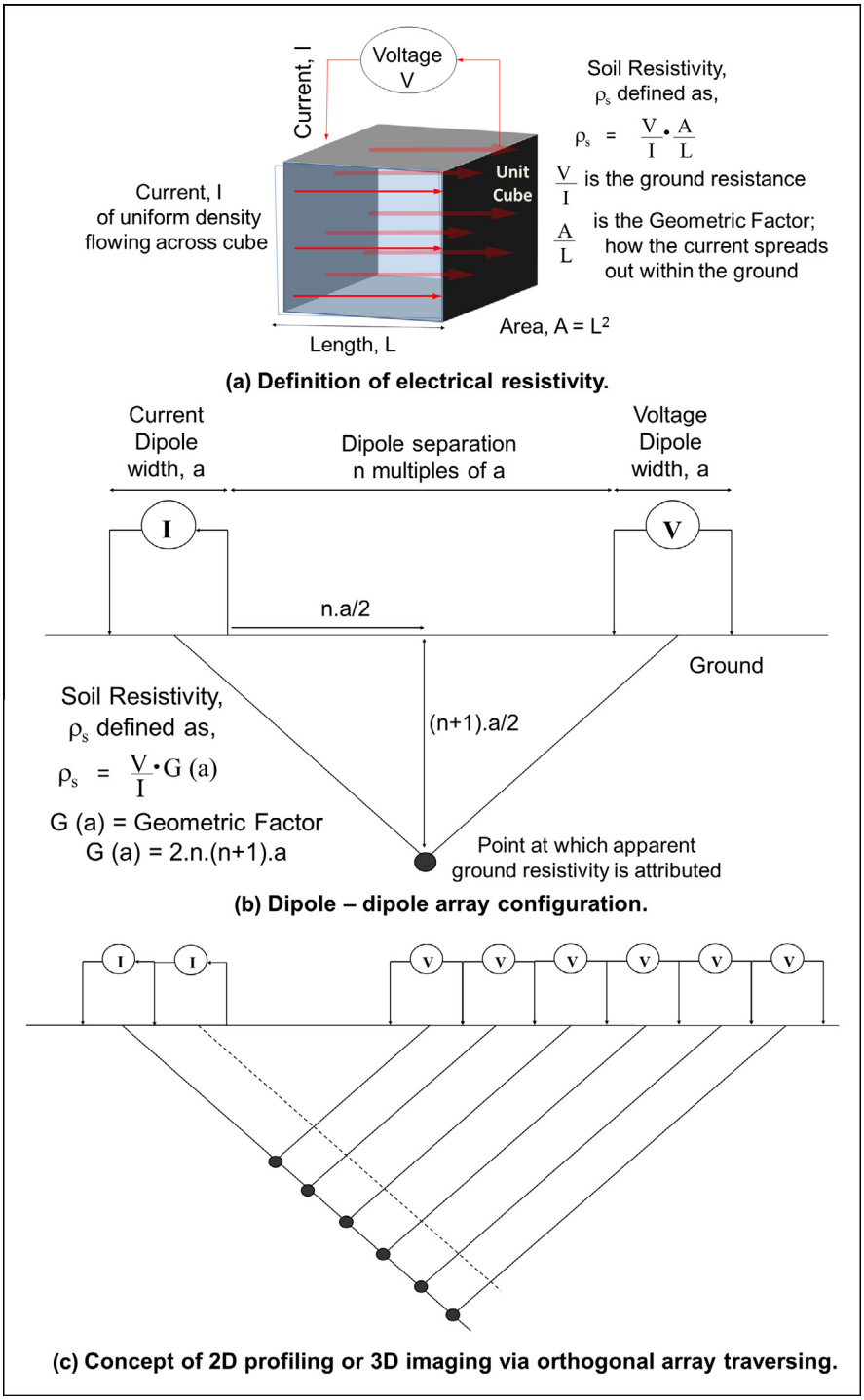

Fig. 1. Resistivity, field surveying arrays and constant separation traversing methods.

databases and web portal access [29,38]. These platforms provide the basis for "smart" technology capable of monitoring the internal physical condition of embankments using diagnostic imaging methods. They operate in the same manner as the field resistivity instruments but are remotely controlled via wireless telecommunications, such as over the mobile phone network. They provide the potential for high-resolution images of subsurface structure, and when used in time-lapse mode, these platforms can monitor groundwater movement and changes in the moisture content of earthworks and surface movement in near real time [37,12]. Hence, these platforms capture information about subsurface processes (groundwater movement) and the resulting spatial and temporal changes in subsurface geotechnical properties, such as moisture content. If we denote these phenomena as the 'CAUSE', we can now access (visualise) information relating to the 'CAUSE' in synchronous with remote, high resolution measurements of surface movement, which we shall denote the 'EFFECT' (or similarly we could apply the term 'SYMPTOM'). Remote access delivers a 'virtual earthworks asset', where the delivery of this information into maintenance decisions, and how it is used to support early interventions, will be core to the development of true preventative maintenance practices (which we develop further in Section 6).

2.2. Resistivity–moisture content relationships

General resistivity ranges for commonly occurring rocks and soils are presented in Fig. 2. While ground resistivity is dependent on the composite soil or rock, it is also controlled by the amount of moisture stored within the pore space and the ionic distribution about grain surfaces (hence the geological materials plotting across a range of resistivities in Fig. 2).

In sands and gravels, the current flows around non-conducting grains via ionic migration within the saturating fluid. A clear relationship has been established between resistivity in sands and gravels and various other factors (Granular: in Fig. 3a), so an accurate measure of resistivity can lead to the calculation of key soil parameters, particularly pore water saturation, and therefore moisture content. This relationship is often termed Archie's Equation [1], where the soil resistivity ρ_s is related to the resistivity of the fluid in the pore space, ρ_w by the degree of saturation, S, i.e. the proportion of the pore space that is filled by the fluid, where $S = 0$ represents completely dry soil (air filled pores) and $S = 1$ represents fully saturated soil (fluid filled pores). Archie's equation also shows that soil resistivity increases with greater compaction (via the compaction factor, 'a' in Fig. 3a), but decreases with increased porosity, n, where the value of the exponent m is related to the grain morphology and how it affects current flow.

Generally, clay resistivity is far lower than granular (e.g. sand and gravel) soil resistivity due to additional matrix conduction caused by the movement of ions distributed across the surfaces of clay particles (clay: in Fig. 3a). Clay resistivity is controlled by both mineralogy and cationic exchange capacity and can also be related to moisture content using established relationships (in Fig. 3a). This relationship was developed by Waxman and Smits [36], where the numerator relates to the ionic migration in the saturating fluid and has a similar form to Archie's Equation, but where the denominator relates to the conduction contribution through the clay matrix. The B parameter relates to the conductance of the cations (such as potassium, calcium, sodium or aluminium) and Q relates to the exchange capacity (CEC) or the capacity for the clay to hold cations within the diffuse double layer about the clay surface (Fig. 3b). For example, higher resistivity clays, such as kaolinite have a low CEC, lower resistivity clays, such as chlorite and illite have a medium CEC and the lowest resistivity clays like smectite have a high CEC. As the plasticity index generally increases with increased CEC, the resistivity ranges for clay dominated mudstones provide not only a very useful index for moisture content but also a very useful proxy for shear strength and thus, resistivity imaging carries the potential to be used to monitor ground strength and stability.

Resistivity has become an important engineering property because it can be used to derive the volumetric moisture content in the calculation of soil moisture deficit (SMD), a standard index of groundwater saturation used in the transportation industry. The railway industry currently uses a simplified calculation of SMD based on regional rainfall using the Meteorological Office Rainfall and Evapotranspiration Calculation System (MORECS). This method provides a broad classification of the network based on a km grid scale and takes no account of either the proportion of precipitation entering the groundwater system or its actual subsurface movement or distribution. However, new geoelectrical imaging-based technologies can provide dynamic 3D images of SMD based on real-time monitoring of the actual moisture movement within infrastructure. Also, resistivity imaging can be used to map the spatial and temporal changes in moisture content, enabling real-time assessment of plasticity changes, for example in response to sustained drought or rainfall.

3. Study sites

Electrical resistivity remote monitoring systems have been installed at two earthworks embankments. Field resistivity data were collected at both sites using the dipole–dipole array configuration (Fig. 1), and apparent resistivity images were inverted using Res2DInv or Res3DInv software [26].

3.1. East Leake site

The East Leake research site comprises a 140 m long section of the whole embankment on the former Great Central Railway (GCR) that extends 800 m. The embankment was built up over the Branscombe Formation of the Mercia Mudstone Group in 1897 using local materials excavated from cuttings to the SW and NE. The material was tipped and then compacted by subsequent movement of shunting locomotives and tipping wagons across the tipped material. The tipping method used along this section of the line was not stated explicitly by Bidder [2], but has been deduced to have been end tipped (e.g. based on historical

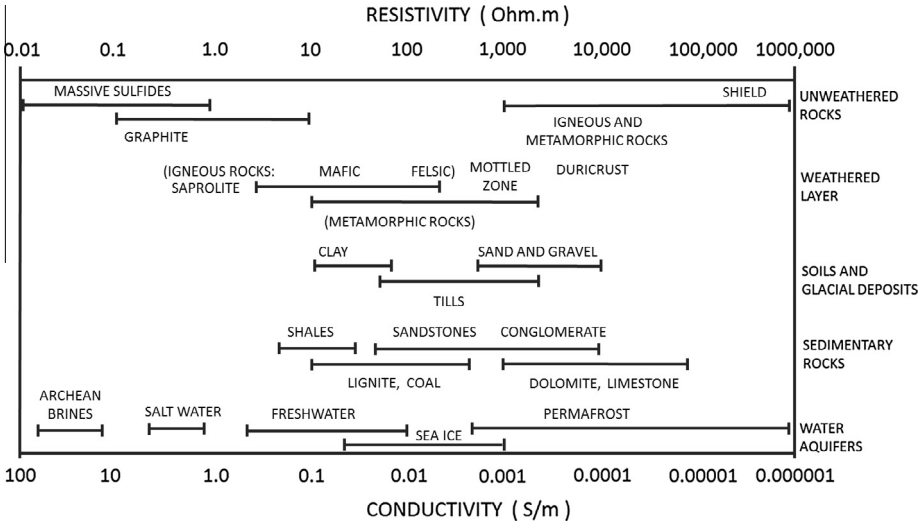

Fig. 2. Resistivity ranges for surface waters, rocks and soils.

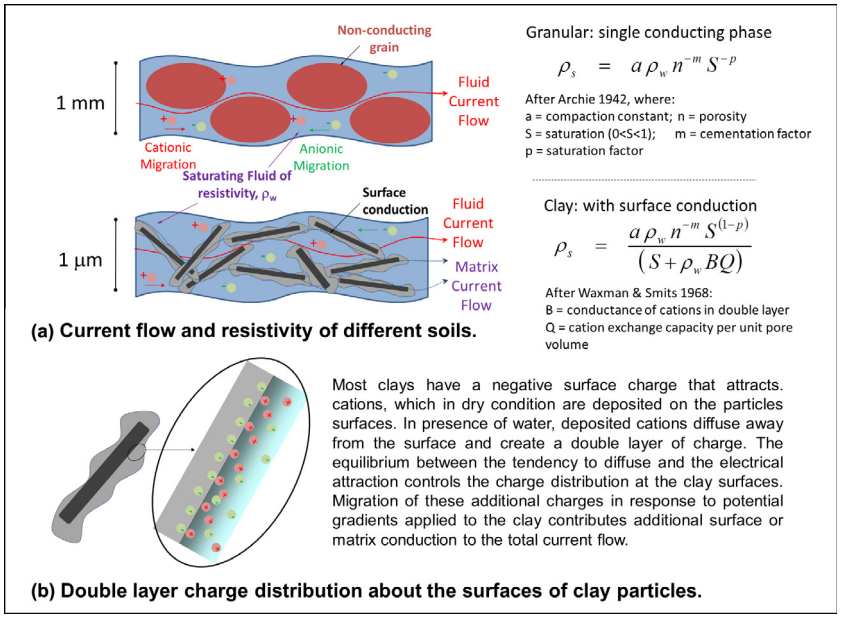

Fig. 3. Moisture content, its effect upon soil charge distribution and resistivity.

photographs taken by S.W. Newton of end tipping wagons and operations in the vicinity of the site at the time of construction). The embankment has been subject to several phases of site investigation spanning from September 2005, which has included drilling, collection of core samples, invasive probing and non-invasive geophysical surveying [16–19,8–11]; borehole locations and the resistivity lines are shown Fig. 4. These phases of SI have shown the embankment to be highly heterogeneous and Gunn et al. [19] provided an interpretation of an along axis section through the test site based upon an interpretation of pits, borehole logs and small strain stiffness profiles, derived from surface wave surveys.

Across the site, soiled modern ballast generally occurs from the surface to around 0.5 m. Immediately underlying the modern ballast in the SE half is the original engineered ballast pavement as described by Bidder [2] and Fox [13] comprising angular granodiorite gravel over granodiorite cobbles. Glaciofluvial sand and gravel occurs beneath the modern ballast over the NE half. The sand is generally uncemented but occasionally the sand was bound within layers around 100 mm thick by fine, white, powdery non-carbonate cement believed to be gypsum leached from other fill materials. Siltstone appears to have been used as an original final dressing to the earthworks fill prior to the laying of the original ballast, but has degraded *in situ* in the embankment. It occurs across much of the section apart from the furthest 30 m in NE end where it is believed to pinch out into the glaciofluvial sand and gravel. All of these materials overlie degraded Late Triassic mudstones that make up the bulk of the earthworks fill either comprising dark grey-black Westbury Mudstone and Clay or red-brown Branscombe Mudstone and Clay.

At East Leake, installations included an array of 64-electrodes spaced at 1.5 m that ran parallel to the west rail ('along-axis' black dashed line in Fig. 4). The electrodes were inserted into a shallow trench that ran along the crest, offset from the rail by approximately 2.5 m, which was excavated with a narrow bucket to approx. 300 mm deep and covered over with ballast. Also, several 32-electrode line arrays were installed across the embankment, each spanning from the toe of the west flank to the toe of the east flank with a 1 m spacing ('cross-axis' blue and red dashed lines in Fig. 4). Along the earthworks flanks, electrodes were installed into a slit cut with a small spade. The positions of these cross-sectional transects were chosen to investigate the effect of different fill materials on the resistivity sections. These lines were installed during July 2006, when a series of resistivity measurements were first

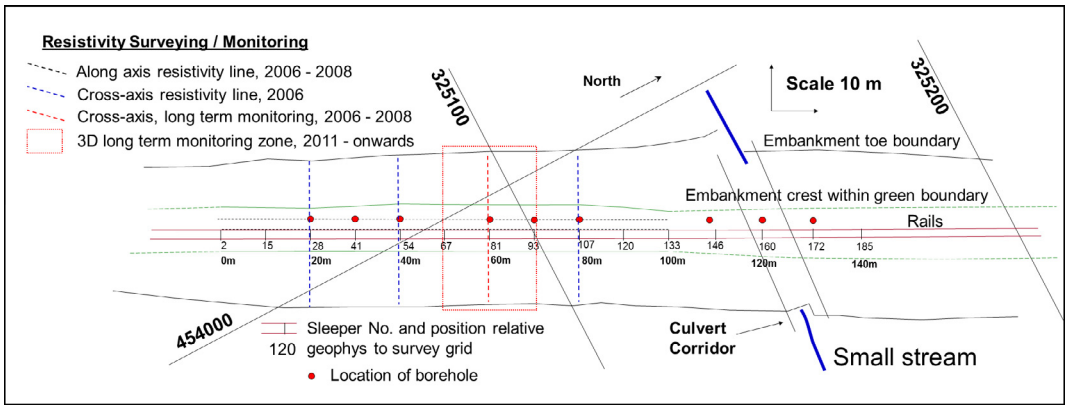

Fig. 4. East Leake: layout of resistivity surveying and monitoring lines on a section of embankment.

made using an AGI SuperSting R8 system. From that time for a period extending into early 2008, repeat measurements were made on the along-axis line and the cross-axis line at the 60 m station at approximately 6 weekly intervals using the same equipment. Measurements were made using the dipole–dipole configuration with current and potential dipole widths (a) of 1–4 times the electrode spacing and unit dipole separations (n) of 1–8.

During September 2010, a permanent resistivity monitoring array was installed within a 22 m section of the embankment, comprising twelve cross-axis lines spaced at 2 m intervals. This 3D zone was approximately centred on the existing cross-axis line at the 60 m station (red dashed line in Fig. 4). The additional lines also comprised 32 electrodes spaced at 1 m intervals, running from the toe of the eastern flank to the toe of the western flank. An ALERT system was also installed at the site at this time, with which measurement schedules were variably programmed to capture (with high temporal resolution) weather event triggered water movement within the embankment. In this way, response to heavy rainfall events could be studied. The system was powered by a combination of solar panel and a methanol fuel cell charging banks of 12 V batteries. Remote monitoring over this 3D array was undertaken over the period from September 2010 to February 2012. A network of proprietary temperature sensors was also distributed in the embankment to depths of 3.7 m, which are used to study the seasonal temperature change patterns throughout the embankment.

4. BIONICS site

The embankment axis is orientated in an east–west direction. It is 90 m long, 6 m high, has a 29 m base width and a 5 m wide crest with 1 in 2 slopes on the flanks. The embankment was constructed in 2005 in four main 18 m-long sections, with the two inner-most sections constructed according to Highways Agency specifications using 0.3 m lifts and 18 passes of a 7.3 tonne self-propelled smooth drum vibrating roller [14,15,20–22]. These have been termed the 'well compacted panels' and simulate new-build highway embankments (Panels B and C in Fig. 5a). The two outer-most sections were built to represent poorly constructed/heterogeneous rail embankments, using four lifts, each nominally of 1.3 m height with minimum tracking by site plant; termed 'poorly compacted' (Panels A and D in Fig. 5a).

To prevent any hydraulic connectivity between each section vertical impermeable membranes were installed during construction between the panels. Immediately after construction the embankment slopes were seeded with grassland seeds typical of the North East of England and other plant species allowed to colonise the embankment naturally. The earthworks fill comprise a sandy, silty clay, which was a locally sourced glacial till (Durham Till) with matrix supported clasts (of greater than coarse gravel size) removed. Atterberg limit tests indicated moisture contents at the Plastic Limit (PL) of 24% w/w (approx. 38% v/v) and Liquid Limit (LL) of 45% w/w (approx. 72% v/v), which classifies the fill material as intermediate plasticity. The dry density of material dried from around the PL is approximately 1.6 Mg/m^3. The crest was capped with a 0.5 m thick layer of basalt ballast.

64 electrodes, spaced at 0.5 m were installed across a 32 m transect from the toe of the north flank to the toe of the south flank (Fig. 5b). In the silty clay earthworks, electrodes were installed into a slit cut with a small spade, while across the crest, electrodes were bedded into bentonite clay that filled 0.3 m deep, fist-sized pits, which were then re-covered with ballast. Proprietary geotechnical sensors including the Decagon 5-TM temperature and moisture content and the MPS-1 water potential (suction) were installed just off-line at depths of 0.5 m and 1 m (below the surface) at three locations on the south and north flanks as shown in Fig. 5b. Installation phases occurred during November 2008 and October 2009 and the period of resistivity measurements on this array extended up to mid-2011. Within this monitoring period, a permanently installed ALERT system was used to make resistivity measurements over this line on a weekly interval. Measurements were made using the dipole–dipole configuration with current and potential dipole widths (a in Fig. 1b) of 1–4 times the electrode spacing (0.5, 1, 1.5 and 2 m) and unit dipole separations (n in Fig. 1b) of 1–8 times the electrode spacing.

5. Surveying and monitoring images

Using the aged, end-tipped embankment and the modern compacted embankment as case histories, this section presents examples of how 2D, 3D and time-lapse resistivity difference images can be used to aid interpretation of embankment structure and condition, and monitor ground water movement processes through the earthworks. Most importantly, these case histories demonstrate the potential for using resistivity as a proxy for the long-term monitoring of geotechnical properties, offering insight into future technology that can provide timely information to support preventative asset maintenance practices.

5.1. 2D static images – material mapping application: East Leake site

The 2D along-axis section provides infill information between boreholes on the subsurface structure to aid interpretation relating to the construction of the embankment (Fig. 6). In Fig. 6a, from the 0 m to the 40 m stations, the resistivity of the interval from 0.8 m to 4 m is generally below 20 Ω m and this is consistent with values that would be expected for clay and mudstone materials. This zone of low resistivity coincides with low stiffness, low penetration resistance zones and relatively high friction ratios, and has been classed as a zone of high moisture and low strength [16,17,19]. The originally tipped fill would have been a coarse gravel comprising lithoclasts predominantly of locally sourced Westbury Mudstone (Fig. 6b). Over the lifetime of the embankment (116 years), the mudstone has weathered to clay and it is believed that this degraded clay material is a key factor in the moisture retention in this zone. From the 40 m to about the 60 m station, the resistivity of the interval from 0.8 m to 4 m is between 20 Ω m and 50 Ω m. This has been interpreted as fill predominantly of gravel comprising Westbury Mudstone, possibly with occasional siltstone from the Blue Anchor Formation. Lower resistivities within this range are consistent with less weathering and less degradation of the mudstone clasts resulting in the earthworks being more freely draining. This zone has been classified as intermediate strength and moisture content, and, represents a buffer between the low strength, mudstone, clay-dominant fill and the high strength, sand, gravel and siltstone-dominated fill. This buffer zone provides the interface between earthworks with very different engineering properties and hence very different performances including response to dynamic loading, drainage, and seasonal variation. From 60 m a lens of fill comprising sand, gravel and siltstone produces a wedge shaped zone with resistivities above 150 Ω m. The wedge develops from the surface at about the 40 m station and thickens to about the 70 m station such that it extends from just beneath the surface to 4 m depth. This high resistivity wedge persists longitudinally under the embankment crest over this depth interval towards the 100 m station. The high resistivity of this zone indicates that the fill has low moisture content and has been shown to be associated with high penetration resistance values and high stiffness values [16,17,19].

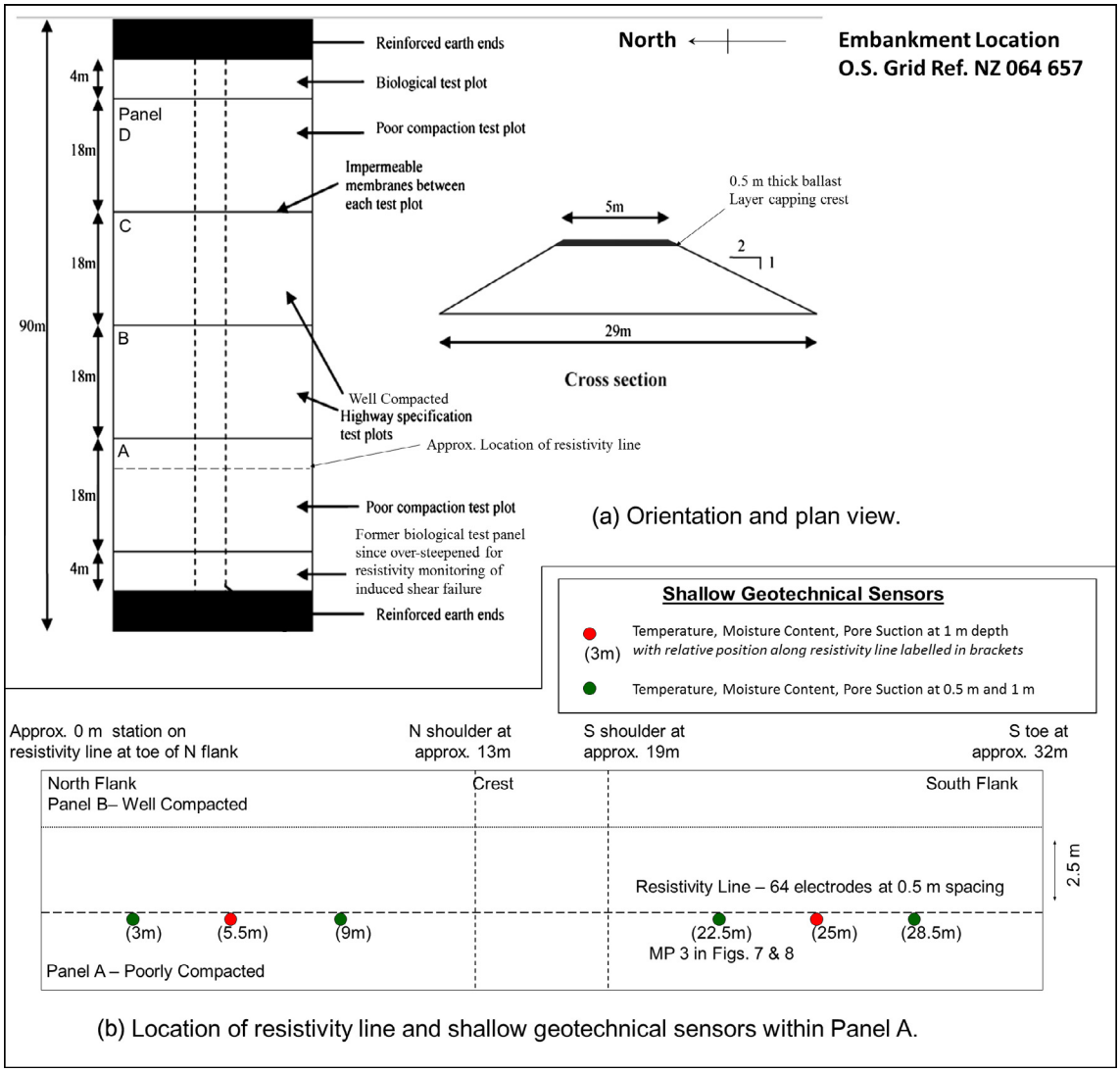

Fig. 5. BIONICS: general structure of embankment and layout of resistivity line in poorly compacted section.

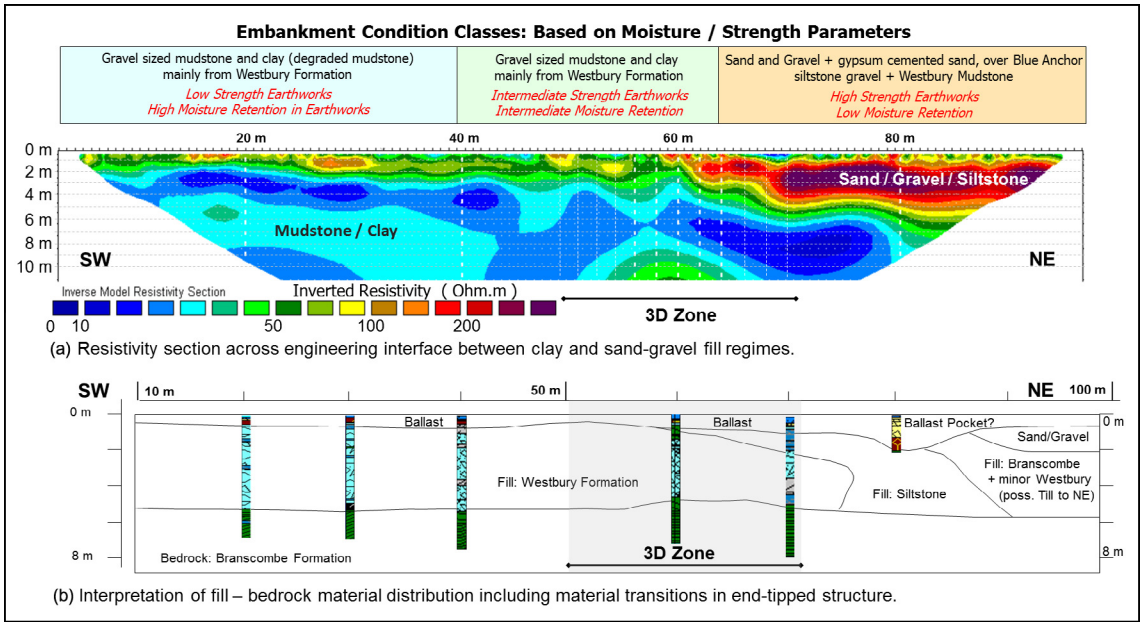

Fig. 6. Structural interpretation and material characterisation aided by 2D 'along-axis' resistivity image.

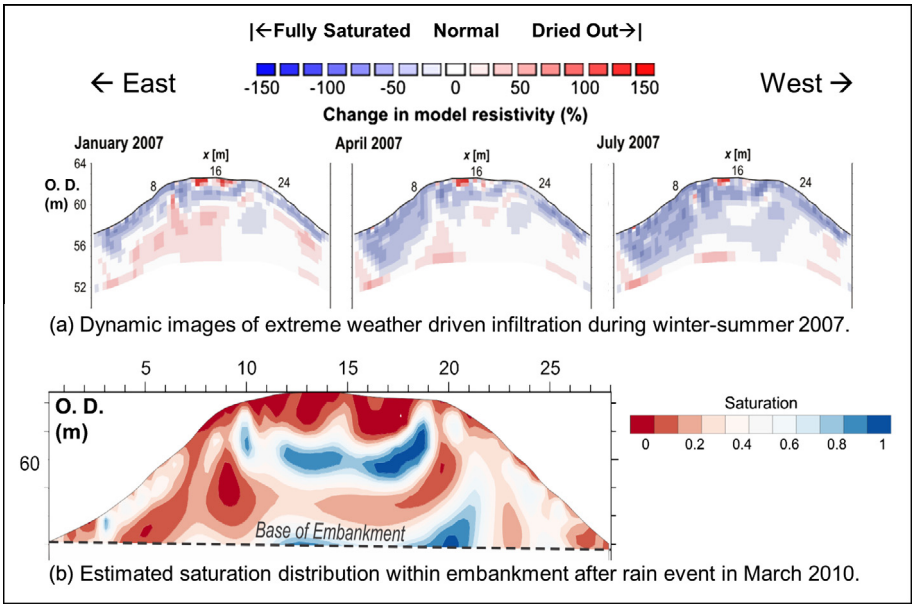

Fig. 7. Imaging moisture movement and moisture conditions within embankment.

5.2. 2D dynamic difference images – groundwater and moisture content changes: East Leake site

Fig. 7 shows how the record-breaking rainfall during the 2007 winter–summer transition was captured by the 6-weekly schedule of resistivity image monitoring on the 'cross-axis' line at the 60 m station. This extreme rainfall event led to the gradual infiltration and near full saturation of the east flank of the embankment (left side). In fact, the infiltration zone extends into the underlying Branscombe Formation, implicating bedrock processes as part of the drainage problem. During these flood events, standing water develops in this area within the cess at the toe of the east flank. While, the embankment at this location shows little sign of climate-induced distress, the sequence of images in Fig. 7a demonstrates how resistivity-differencing between images can be used to monitor build up of potentially unstable moisture conditions. Chambers et al. [12] describe methods of temperature correction and development of moisture content–resistivity relationship for the Westbury Formation fill materials at the East Leake site. The relationship is based upon fitting the Waxman-Smits [36] relationship (Fig. 3a) to a series of resistivity measurements on dried samples that were reconstituted to a range of known moisture contents. Based on this resistivity-moisture content transformation, Fig. 7b provides an imaged estimate of the saturation distribution throughout the embankment after a heavy rain event on 30th March, 2010. The key features of note include: the infiltration into the east and west flanks (which appears greater on the east flank) and the highly saturated central core of the embankment, which is believed to partly associated with perching over an interval of clay degraded from the Westbury Mudstone. In the context of early intervention, the high levels of saturation may be sufficient to classify this location as at risk, requiring monitoring that could be achieved via remote delivery of saturation images on a weekly or even daily basis from a temporary retrofitted electrode array. The monitoring period would then be sufficient to capture the full extremes of weather events affecting the site. The temporal and spatial characteristics of the groundwater movement would be investigated using a series of time-lapse images and used to plan future drainage schemes.

5.3. 2D dynamic difference images – moisture content and pore suction changes: BIONICS site

Fig. 8 shows a series of six resistivity images across the BIONICS embankment captured from spring to summer of 2009 when air temperatures regularly exceeded 20 °C during May and June. During this time there was little significant rain until a series of weather events that brought rainfall that occurred in June and July. The layered structure in the resistivity sections can be attributed to the sequence of lifts and ballast capping employed during the construction of this poorly compacted section of embankment, where Table 1 summaries the broad resistivity and geotechnical properties of the layers identified.

The ballast cap at the top of the embankment (Layer 1) exhibits the largest resistivities to 800 Ω m. The underlying silty clay in Layer 2 exhibits the lowest resistivities of below 10 Ω m. Low resistivity zones occur at the interface between Layer 2 and the overlying ballast, where infilling of the ballast cap into a depression is observed beneath the northern half of the embankment crest. The low resistivities in layer 2 below this structure would result from perching of rainwater that drains through the ballast. The clay fill in this zone would be soft, being above its PL (possibly approaching its LL) and of low strength ≅ 10 kPa. Notably, Layer 3 is highly resistive, indicating a high strength clay with moisture contents well below the PL. The moisture contents in Layer 4 and the underlying zones appear to close to the expected in situ moisture levels and show little variation during this monitoring period.

This series of images capture the property change domains within the embankment associated with it drying out in response to relatively low rainfall and a seasonal increase in temperature from the spring to summer 2009. The resistivity difference images (between the baseline image on 14th March and the 1st May, 1st June) indicate the resistivity change distribution throughout the embankment, and thus provide insight into the exfiltration process. Note that the resistivity of Layer 2 appears to decrease and Layer 3 increase during this period, which could be related to a wicking suction due to evaporation from the ballast cap. However, the most significant increase in resistivity (as high as 10 times) occurred in the upper 0.75 m interval of the south flank. During this drying event, the ground temperature rises from

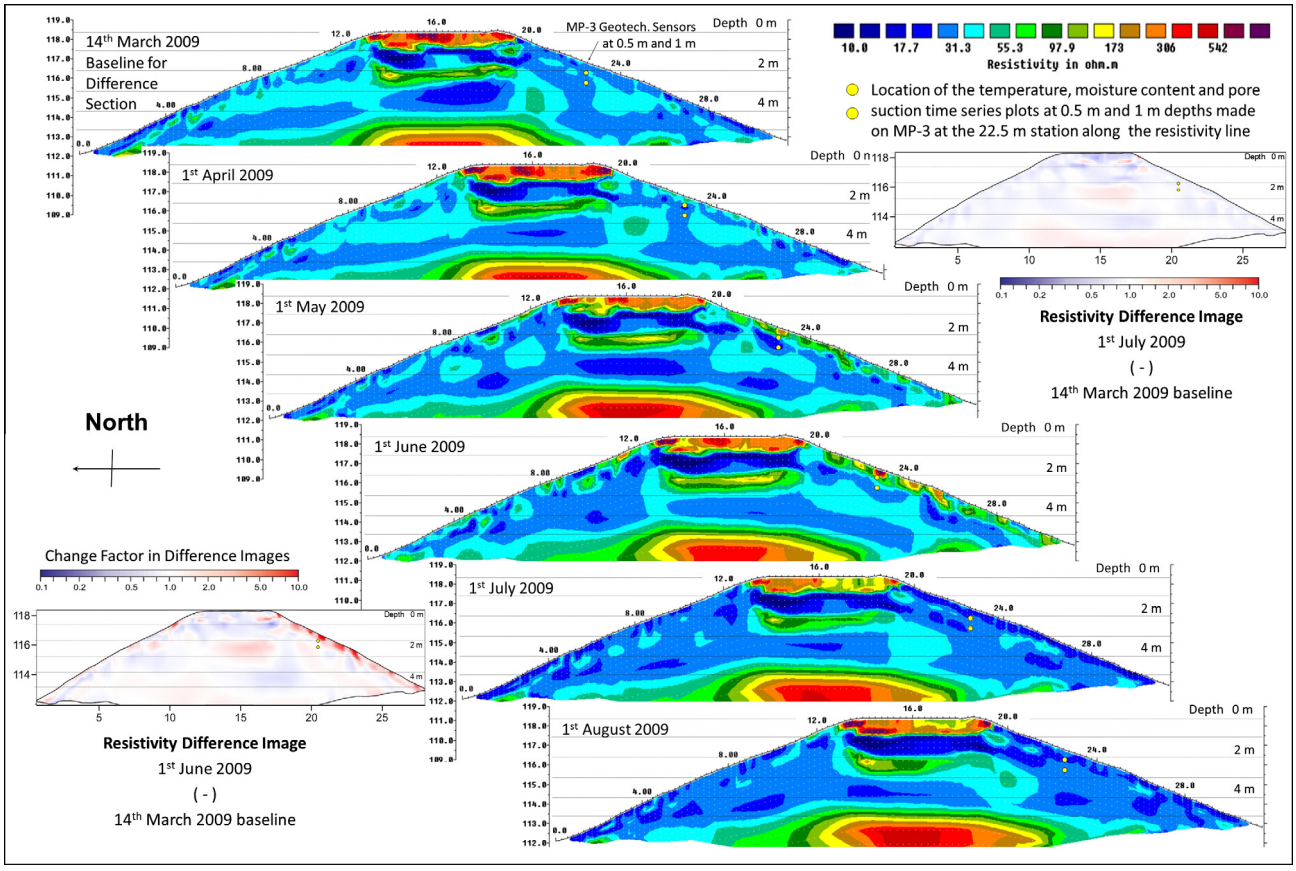

Fig. 8. BIONICS: resistivity image differences during drying event of spring–summer 2009.

Table 1
Resistivity and estimated geotechnical property ranges of the BIONICS embankment layers.

Structure			Geophys	Estimated geotechnical property ranges		
Layer no.	Depth interval (m)	Main fill lithology	Resistivity range (Ω m)	Moisture content range (% v/v)	Plasticity	Shear strength (kPa)
1	0–1	Ballast	800–170			
2	1–2	Clay	40–<10	25–80	<PL→LL	100–10
3	2–3	Clay	170–50	5–20	≪PL	≫100
4	3–4	Clay	30–20	30–45	→PL	⩾100
5	>4	Clay	>30[a]	<30	<PL	>100

PL – Plastic Limit, LL – Liquid Limit.
[a] Images have lower sensitivity in centre of embankment at depth.

around 6 °C (6 °C) in March to above 14 °C (12 °C) in June at 0.5 m (1 m) depths, (Fig. 9).

During early March, the moisture content sensor recorded 40%v/v (37%) and the pore suction was at its limit of suction of −10 kPa (−10 kPa) at 0.5 m (1 m) depths. Changes in the moisture content and pore suction measurements during drying throughout late March to early June to 26%v/v (34%) and −480 kPa (−270 kPa) at 0.5 m (1 m) show how the moisture loss and development of suction pervades from the surface into the embankment. Lowest moistures and greatest suctions were recorded on 8th June prior to a series of weather systems that brought steady rainfall, the first of which occured from 9 to 11 June. Recharge into the embankment reverses results in an increase in the measured moisture content and a decrease in suctions. There is a more immediate and greater magnitude of response at 0.5 m than at 1 m, again demonstrating how infiltration is driven by recharge from the surface. Note how the later rainfall events during 22–26 June and 29 June–4 July resulted in a loss of suction and higher moisture contents in July than in March. These events provided sufficient rain to produce lower resistivities across the whole of the embankment in the upper 0.5–1 m interval (resistivity difference image between 1st July and 14th March).

5.4. 3D Dynamic images – process and property change visualisation

The comparison of time series data with dynamically changing 2D or 3D images demonstrates the challenge of up-scaling from a single point sensor to the whole asset. Although it is common practice to monitor earthworks using point sensors, it is very difficult to fully quantify the processes driving property changes (i.e. magnitude and rate of spatial change) without a dynamic, volumetric visualisation of those properties throughout the whole earthworks asset. Full volumetric visualisation can be provided by a 3D image, but while technologies for direct, non-invasive geotechnical property imaging are scarce (or if they exist at all), resistivity-based proxy images to moisture content and even pore suction are possible

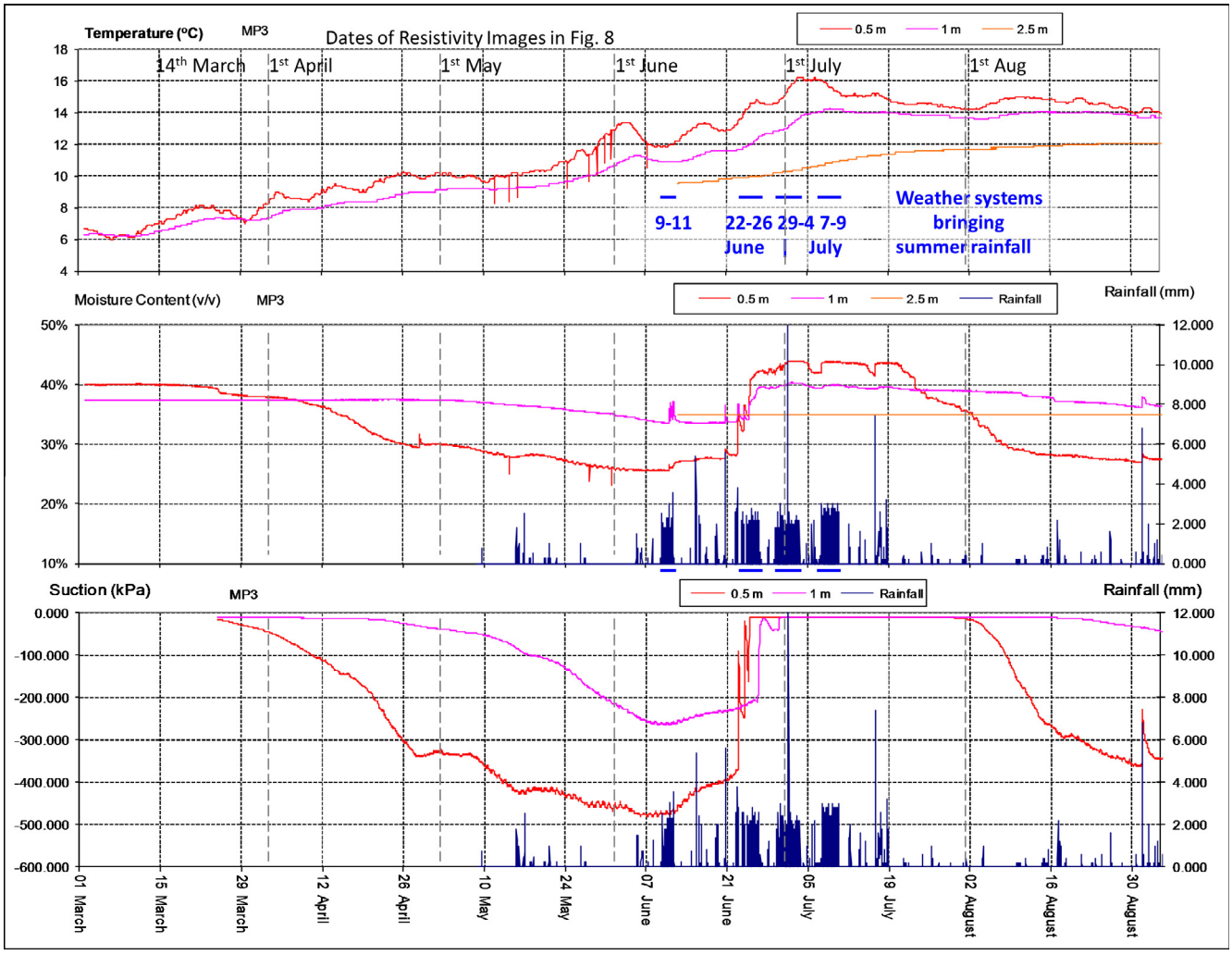

Fig. 9. Temperature, moisture content and pore suction time series at MP-3 0.5 and 1 m depths during spring–summer 2009 drying event.

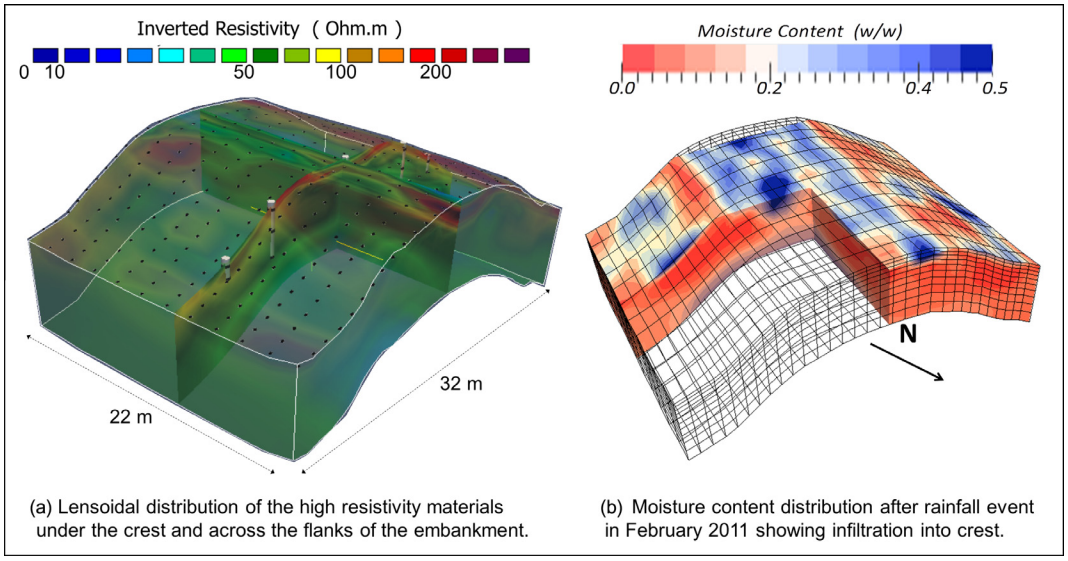

Fig. 10. 3D resistivity and derived geotechnical 'proxy' property distributions in aged Victorian earthworks, (after [12]).

provided sufficiently robust relationships exist between these properties. 3D resistivity images are very easily realised by electrode arrays over a surface area, such as by using a number of parallel line arrays as was the case at East Leake. The resistivity-moisture content relationship used for interpreting the 2D sections can also be applied to 3D images, such as shown in Fig. 10.

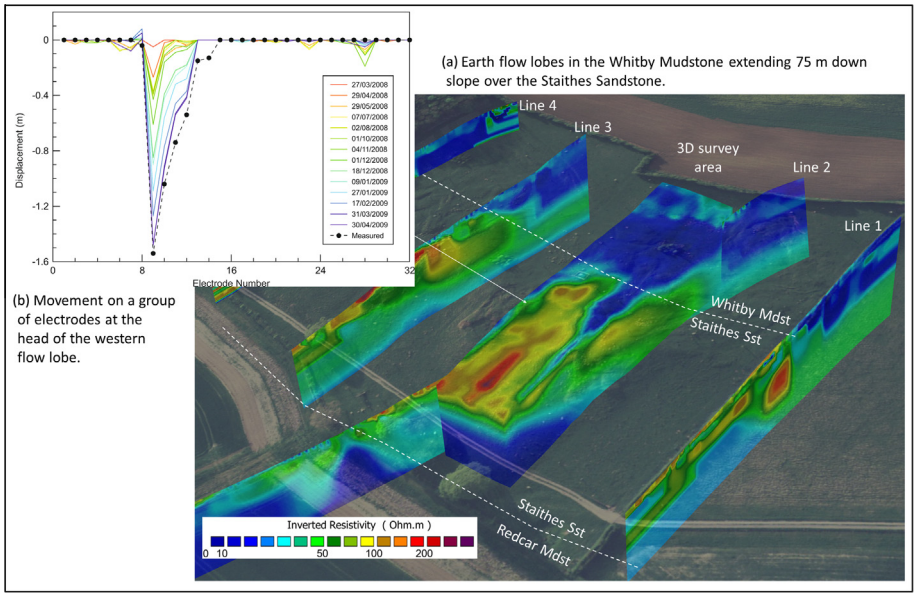

Fig. 11. Resistivity image and movement monitoring on earth flow landslide.

The central along-axis 2D section (non-transparent) in Fig. 10a features the proportion of the section shown in Fig. 6 between the intermediate and higher strength zones. Fig. 10b shows the moisture content distribution after a minor rainfall event in February 2011. While, much of the crest is at high moisture content, very high moisture zones can be observed, such as centre crest on the east–west cutaway. Also, shallow zones of very high moisture on the flanks probably indicate gaps in the vegetation cover. While SMD indices based on MORECS data can be usefully applied for regional assessment of risk to rail infrastructure, their application at site scale is not appropriate if the true variability relating to infiltration and recharge of groundwater into geotechnical asset is not captured. Whereas resistivity or moisture content images can be readily converted into images of SMD simply via knowledge of the fill resistivity at saturation. Indeed, the saturation index used in Fig. 7 provides a proxy to SMD (and it is highly likely that volumetric moisture content and saturation are more valuable indices for characterising the true distribution of internal conditions of earthworks assets).

6. Discussion

Fundamentally, these case histories demonstrate that the construction method, deterioration history and distribution of composite materials within the embankment control engineering performance, especially, the spatial and temporal variation of groundwater and its influence upon key geotechnical properties controlling strength and stability. They relate to end members of a spectrum of engineered embankments. BIONICS, a modern clay embankment that was built up in layers, which are clearly recognised within the resistivity images. East Leake, an aged embankment with a heterogeneity that reflects the transition of a range of fill materials within an end tipped structure, again, identified on resistivity images. These case histories also demonstrate the application of time lapse resistivity images in understanding the link between weather events and subsurface processes and property changes affecting stability, which if applied to a 'virtual asset' provide the potential for predictive maintenance, for example within the context of resilient infrastructure in future climates.

The BIONICS example provides insight into how seasonal, cyclic wetting and drying in the near surface could drive the development of fissure networks deeper into the flank. For example, one can envisage similar processes driving the progressive moisture-driven cyclic strains and development of zones of low shear strength that could comprise long term instability due to shear failure. In addition to this holistic visualisation of the subsurface driving processes, recent innovations in time lapse, differential resistivity image processing now enable automated systems to track the movement of the individual sensors within the monitoring network [37,38]. We can now establish cause and effect between coupled subsurface and surface processes in rapid ground failure events. While we have not yet applied this technique to our engineered embankment sites, we have monitored up to 1.6 m of down slope movement on sensor groups at the top of a natural earth flow lobe with sixteen measurements over one year (inset in Fig. 11). This example relates to a landslide monitoring site near Malton, North Yorkshire where we have imaged the movement and break up of prograding earth flow lobes transporting reworked Whitby Mudstone over the underlying Staithes Sandstone (Fig. 11). The resistivity image clearly maps out the flow of the Whitby Mudstone (blues–greens) over the underlying Staithes Sandstone (yellows–reds).

So, how could we apply these technologies to the management of earthworks assets? We can envisage programmable sequenced images resulting from remote field monitoring on permanent or semi-permanent installations telemetered and stored on a central database that contains multiple sites. These images would be processed to provide 2D, 3D and in time-lapse mode 4D images of resistivity, which are then transformed using robust relationships into geotechnical property ranges (moisture content, pore pressure, etc.). These property distributions would then be interrogated, for example to identify and classify internal infrastructure regimes. There can be multiple threshold levels set, for example, moisture content ranges could, for the basis of identifying regimes, include:

i. Dry: below Shrinkage Limit, [Serviceability Limit State (SLS) – Monitor Subsidence].
ii. No Warning: between Shrinkage and Plastic Limits.
iii. Inspect: between Plastic and Liquid Limits, [SLS – Monitor moisture levels; design drainage].
iv. Wet: above Liquid Limit, [Ultimate Limit State – install drainage systems].

This information could form the basis for new proactive 'On-Demand' asset inspection scheduling. Automatic alarms could be programmed into the system that would issue a series of traffic light warnings that trigger certain actions. For example, the potential for shrinkage and crack formation in those zones triggering a 'Dry' warning could be monitored, either using independent systems or the resistivity based electrode movements. The subsurface image sequences could also map the rate and extent of drying and subsidence for use in considering the effect of vegetation and planning remedial actions (pollarding, etc.). As another example, zones triggering an 'Inspect' warning may indicate potential for plastic deformation (ballast pocket formation, mud pumping or even shear failure, etc.). Again, resistivity images would assist in monitoring moisture levels, movement pathways, sumps, springs, etc. and the subsequent design and scheduling of drainage measures. The detailed visualisation of subsurface ground water movement will enable design of lower cost measures that are better adapted to the specific causes of the problems – these are the subsurface processes. A consequence of responsive mode maintenance strategies is the use of surface based observations that currently define or diagnose the problem via the surface manifestations of the true cause, which is in fact, driven by the subsurface processes. By adopting subsurface imaging technology, we not only better define the cause of the problem (c.f. our use of 'CAUSE' in the East Leake case history hopefully captured the reader's attention), but more importantly, we also buy back a significant period of time in which to consider our early intervention. This is because the true cause of the problem begins as a progressive subsurface process, which could be very manageable if the subsurface symptoms are identified and enable robust prediction of future consequences, sufficient for appropriate preventative actions to be taken. All of this time advantage is lost by waiting for symptomatic surface manifestations, which are usually observations of direct surface movement, and hence maintenance is completely responsive, dealing only with the effect. Currently, the lack of understanding of the information potentially available from subsurface monitoring presents a key barrier inhibiting the development of preventative maintenance. Note also, responsive approaches may not address the true cause of the problem that if untreated, is left to continue to cause the problems. In this way we become trapped in a cycle of responsive maintenance, increasing whole life cycle costs, and quite possibly contributing to a reduction in the total lifespan of the asset.

Finally, by way of conclusion we provide a concept for a possible future linear route warning system. We envisage simple line arrays of electrodes, spaced between 2 m and 10 m extending along a 200 m–1 km long embankment. Two separate sets of monitoring measurements are made along the Up and Down line arrays. We have the capability to produce sequenced resistivity sections along these linear arrays that provide moisture content levels within depth intervals in the lower embankment, embankment core and possibly the upper embankment, again with independent sections for either flank of the asset. Under normal

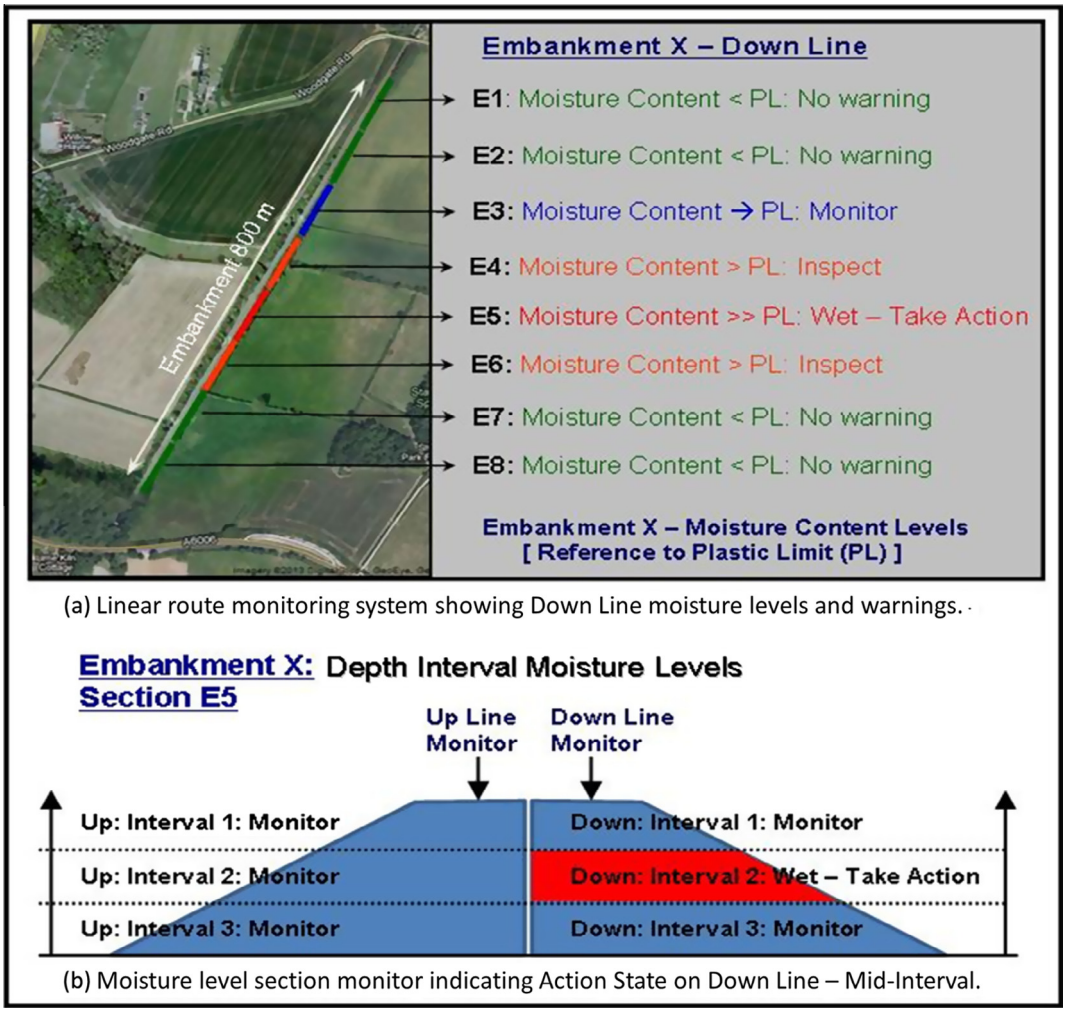

Fig. 12. Concept for a moisture monitoring system based upon real-time resistivity measurements over linear arrays along the Up and Down lines.

operating conditions, moisture level information is updated on a routine monitoring schedule, and these data are interrogated against a series of threshold classes such as the four above. The same routine monitoring schedule is maintained until certain weather event sequences trigger an 'Inspect' along a specific section (see Fig. 12). The warning also indicates the depth interval over which the high moisture levels occur, hence guiding impromptu inspection. This alarm also triggers a reconfiguration of the monitoring schedule, for example reducing the time interval between measurements for the purposes of studying potential temporal and spatial evolution of increased moisture levels. Having established the aerial and depth extent of the affected area, a scheme for drainage intervention is designed and scheduled for installation. Months (years?) later, the maintenance crews are mobilised for installation who don't observe any major surface expressions of distress but note seeping from pit walls at the intervals where the drainage measures are to be installed. By this time, the Inspect warning has been upgraded to 'Wet' – at ultimate limit state condition.

Acknowledgements

This paper is published with the permission of the Executive Director of the British Geological Survey (NERC). The authors gratefully acknowledge the Great Central Rail (Nottingham) Ltd. for allowing access to site and the publication of this manuscript.

References

[1] Archie GE. The electrical resistivity log as an aid in determining some reservoir characteristics. Petroleum Trans AIME 1942;146:54–62.
[2] Bidder FW. The great central railway extension: Northern division. ICE, Vol. CXLII, Session 1899–1900, Part IV, Paper 3227, 1900. p. 1–22.
[3] Bouch C, Jaroszweski D, Baker C, Dijkstra T, Dingwall R, Dixon N, Ryley T, Sivell P, Gunn D, Lawley, R. Future Resilient Transport Networks (FUTURENET): an overview of the FUTURENET project with particular reference to railway aspects. World Congress on Rail Research, 22–26 May 2011, Lille.
[4] Bouch C and others incl., Gunn DA, Lawley R. Future resilient transport networks (FUTURENET): assessing transport network security in the face of climate change. In: 91st annual meeting of the transportation research board, January 22–26, 2012, Washington, DC.
[5] Brough M, Stirling A, Ghataora G, Madelin K. Improving railway subgrade stiffness – assessment of traditional in situ ground improvement techniques. In: Proc. 3rd Int. Con. Railway Engineering, London; 2000.
[6] Brunet P, Clement R, Bouvier C. Monitoring soil water content and deficit using Electrical Resistivity Tomography (ERT) – a case study in the Cevennes area, France. J Hydrol 2010;380:146–53.
[7] Cassiani G, Godio A, Stocco S, Villa A, Deiana R, Frattini P, et al. Monitoring the hydrologic behaviour of a mountain slope via time-lapse electrical resistivity tomography. Near Surf Geophys 2009;7:475–86.
[8] Chambers JE, Gunn DA, Wilkinson PB, Ogilvy RD, Ghataora GS, Burrow MPN, Tilden Smith R. Non-invasive time-lapse imaging of moisture content changes in earth embankments using Electrical Resistivity Tomography (ERT). In: Ed. Ellis E, Yu HS, McDowell G, Dawson A., Thom N, editors. Advances in Transportation Geotechnics. Proc. 1st int. conf. transportation geotechnics, Nottingham, August 2008. p. 475–480.
[9] Chambers JE, Gunn DA, Weller AL, Kuras O, Wilkinson PB, Meldrum PI, Ogilvy RD, Jenkins GO, Gibson AD, Ford JR, Price SJ. Geophysical anatomy of the Hollin Hill Landslide, North Yorkshire, UK. In: 14th European meeting of environmental and engineering geophysics, Krakow, Poland, 15–17 September, 2008.
[10] Chambers JE, Gunn DA, Meldrum PI, Wilkinson PB, Ogilvy RD, Haslam E, Holyoake S, Wragg J. Volumetric monitoring of earth embankment internal structure and moisture movement as a tool for condition monitoring. In: Proc. 11th int. conf. railway engineering, London; 2011.
[11] Chambers JE, Wilkinson PB, Kuras O, Ford JR, Gunn DA, Meldrum PI, et al. Three-dimensional geophysical anatomy of an active landslide in Lias Group mudrocks, Cleveland Basin, UK. Geomorphology 2011;125:472–84.
[12] Chambers JE, Gunn DA, Wilkinson PB, Meldrum PI, Haslam E, Holyoake S, et al. 4D electrical resistivity tomography monitoring of soil moisture dynamics in an operational railway embankment. Near Surf Geophys 2014;12(1):61–72.
[13] Fox FD. The great central railway extension: Southern division. ICE, Vol. CXLII, Session 1899–1900, Part IV, Paper 3209, 1900, p. 23–48.
[14] Glendinning S, Rouainia M, Hughes P, Davies O. Biological and engineering impacts of climate on slopes (BIONICS): the first 18 months. Int. Assoc. Eng. Geol., Nottingham, Paper 348; 2006.
[15] Glendinning S, Loveridge F, Starr–Keddle RE, Bransby MF, Hughes PN. Role of vegetation in sustainability of infrastructure slopes. In: Proceedings of the institution of civil engineers, engineering sustainability, 2009, 162, No. 2, p. 101–110.
[16] Gunn DA, Reeves H, Chambers JE, Pearson SG, Haslam E, Raines MR, Tragheim D, Ghataora G, Burrow M, Weston P, Thomas A, Lovell JM, Tilden Smith R, Nelder LM. Assessment of embankment condition using combined geophysical and geotechnical surveys. In: Proc. 9th int. conf. railway engineering, London; 2007.
[17] Gunn DA, Reeves H, Chambers JE, Ghataora G, Burrow M, Weston P, Lovell JM, Tilden Smith R, Nelder LM, Ward D. New geophysical and geotechnical approaches to characterise under utilised earthworks. In: Proc. 1st int. conf. transportation geotechnics, Nottingham; 2008.
[18] Gunn DA, Haslam E, Kirkham M, Chambers JE, Lacinska A, Milodowski A, Reeves H, Ghataora G, Burrow M, Weston P, Thomas A, Dixon N, Sellers R, Dijkstra T. Moisture measurements in an end-tipped embankment: Application for studying long term stability and ageing. In: Proc. 10th int. conf. railway engineering, London; 2009.
[19] Gunn DA, Raines MG, Chambers JE, Haslam E, Meldrum PI, Holyoake S, Kirkham M, Williams G, Ghataora GS, Burrow MPN. Embankment stiffness characterisation using MASW and continuous surface wave methods. In: Proc. 11th int. conf. railway engineering, London; 2011.
[20] Hughes P, Glendinning S, Mendes J. Construction Testing and Instrumentation of an infrastructure testing embankment. In: Proc. expert symposium on climate change: modelling, impacts & adaptations, Singapore; 2007. p. 159–66.
[21] Hughes PN, Glendinning S, Davies O, Mendes J. Construction and monitoring of a test embankment for evaluation of the impacts of climate change on UK transport infrastructure. In: Proc. 1st int. conf. transportation geotechnics, Nottingham; 2008.
[22] Hughes PN, Glendinning S, Mendes J, Parkin G, Toll DG, Gallipoli D, Miller P. Full-scale testing to assess climate effects on embankments. Special issue of engineering sustainability, Institution of Civil Engineers, 162, No. ES2, 2009, p. 67–79.
[23] IPCC. Intergovernmental panel on climate change: synthesis report. In: Pachauri RK, Reisinger A, editors. Contribution of working Groups I, II and III to the fourth assessment report. Cambridge Univ. Press: Cambridge, UK; 2007. 104p.
[24] IPCC. Climate Change 2007: Impacts, Adaptation and Vulnerability. In: Parry ML, Canziani OF, Palutikof JP, van der Linden PJ, Hanson CE, editors. Contribution of working Group II to the Fourth assessment report of the intergovernmental panel on climate change. Cambridge University Press: Cambridge, UK; 2007. 976 p.
[25] Li D, Selig ET. Evaluation of railway subgrade problems. transportation research Record No. 1489, Rail, Transportation Research Board, Washington, DC; 1995. p. 17–25.
[26] Loke MH. RES2DINV Rapid 2-D resistivity and IP inversion using the least-squares method. Manual, Geotomo Software, Penang, Malaysia; 2006.
[27] Niesner E. Subsurface resistivity changes and triggering influences detected by continuous geoelectrical monitoring. The Leading Edge, August 2010. p. 952–55.
[28] O'Brien AS. Rehabilitation of urban railway embankments – investigation, analysis and stabilisation. In: Cuellar V, Dapene E et al., editors. Proceedings of XIV European conference on soil mechanics and geotechnical engineering, Madrid, September 2007.
[29] Ogilvy RD, Meldrum PI, Kuras OA, Wilkinson PB, Chambers JE. Advances in geoelectrical imaging technologies for the measurement and monitoring of complex earth systems and processes. In: 33rd int. geol. congress, Oslo; 2008.
[30] Ogilvy RD, Meldrum PI, Kuras O, Wilkinson PB, Chambers JE, Sen M, et al. Automated monitoring of coastal aquifers with electrical resistivity tomography. Near Surf Geophys 2009;7:367–75.
[31] Okada K, Ghataora GS. Assessment of the stiffness of railway subgrade. In: Proc. 3rd int. con. railway engineering, London; 2000.
[32] Reeves GM, Sims I, Cripps JC. Clay materials used in construction. Geological Society Engineering Geology Special Publication No. 21; 2004. 517p.
[33] Selig ET, Waters GM. Track geotechnology and substructure management, Thomas Telford; 1994. 446p.
[34] Shevnin V, Mousatov A, Ryjov A, Delgado-Rodriquez O. Estimation of clay content in soil based on resistivity modelling and laboratory measurements. Geophys Prospect 2007;55:265–75.
[35] Sjodahl P, Dahlin T, Johansson S. Using the resistivity method for leakage detection in a blind test at the Rossvatn embankment dam test facility in Norway. Bull Eng Geol Environ 2010;69:643–58.
[36] Waxman MH, Smits LJM. Electrical conductivities in oil-bearing shaly sands. Soc Petrol Eng J 1968;8:107–22.
[37] Wilkinson PB, Chambers JE, Meldrum PI, Gunn DA, Ogilvy RD, Kuras O. Predicting the movements of permanently installed electrodes on an active landslide using time-lapse geoelectrical resistivity data only. Geophys J Int 2010;183:543–56.
[38] Wilkinson PB, Chambers JE, Kuras O, Meldrum PI, Gunn DA. Long-term time-lapse geoelectrical monitoring. The First Break 2011;29:77–84.